Nanofluidic fluorescence microscopy with integrated concentration gradient generation for one-shot parallel kinetic assays

Pattamon Teerapanich, Martine Pugniere, Corinne Henriquet, Yii-Lih Lin, Antoine Naillon, Pierre Joseph, Chia-Fu Chou, Thierry Leichle

Nanofluidic fluorescence microscopy with integrated concentration gradient generation for one-shot parallel kinetic assays

Pattamon Teerapanich[a], Martine Pugnière[b], Corinne Henriquet[b], Yii-Lih Lin[c], Antoine Naillon[d], Pierre Joseph[a], Chia-Fu Chou[c], and Thierry Leïchlé[a,*]

[a]LAAS-CNRS, Université de Toulouse, CNRS, Toulouse, France

[b]IRCM, Institut de Recherche en Cancérologie de Montpellier, INSERM, U1194, Université de Montpellier; ICM, Institut Régional du Cancer, Montpellier, F-34090 France

[c]Institute of Physics, Academia Sinica, Taipei 11529, Taiwan

[d]CNRS, IMFT, F-31400 Toulouse, France

***Corresponding author**

Email address: tleichle@laas.fr (T. Leïchlé)

Abstract

We report a simple and cost-effective nanofluidic fluorescence microscopy platform with parallel kinetic assay capability for the determination of kinetic parameters in a single run. An on-chip microfluidic concentration diluter, or gradient generator, was integrated to a biofunctionalized nanofluidic chip, enabling simultaneous interrogation of multiple biomolecular interactions with a full titration series of analyte in a single experiment. We demonstrate that since the association and dissociation phases are induced by the on-chip gradient generator and a reverse buffer flow operation, complete kinetic sensorgrams for IgG/anti-IgG interactions can be achieved within 20 min on a single device, which is at least 10 times faster than traditional kinetic techniques. This method could contribute to low-cost, rapid and high-throughput drug-screening and clinical diagnostics.

Introduction

High-throughput measurement of biomolecular interactions with rapid determination of the affinity and kinetic parameters are of critical importance in drug discovery processes and proteomic analysis.[1] Surface plasmon resonance (SPR) is established as a powerful bioanalytical tool for quantitative characterization of molecular binding events owing to its real-time and label-free detection.[2] Traditional kinetic experiment requires the successive introduction of different analyte concentrations and the sensor surface is regenerated after each analyte injection, a protocol regarded as “multi-cycle kinetics”. These repetitive procedures are typically performed manually, and thus are laborious and time-consuming.

Over the past decade however, single cycle titration kinetic was implemented on SPR to decrease the number of regeneration steps: FastStep[3] and diSPR®[4] dynamic injections are now commercialized in the PIONEER FE SPR instrument, mainly used in drug screening[5]. Moreover, there has been a growing interest in high-throughput kinetic analysis using SPR imaging (SPRi) technology as demonstrated in

the commercial cross-flow ProteOn XPR 36 assay system (BioRad),[6] or the flow cell based FlexChip (Biacore).[7] Combined with protein arrays, SPRi uses a parallel detector such as a CCD camera to measure kinetics on multiple ligand surfaces in a single run without the need of surface regeneration. In the near future, SPR microscopy[8] and emerging SPR systems based on nanostructures[9] which propose higher throughput and sensitivity, could also stimulate the field.

Despite the capability to provide kinetic data in a parallel manner, the above mentioned systems necessitate a high-cost specialized optical instrument and specifically trained operators.[10] On the other hand, electrochemical and quartz crystal microbalance biosensors may provide low-cost solution for kinetic studies,[11,12,13] but they encounter the similar issues, as SPR platform, of either sensor surface regeneration,[14] difficulty in parallel kinetic assays,[15] or slow assay time, particularly when target concentrations are close to the sensor detection limit,[16,17] for kinetic analysis, though the later can be alleviated by implementing complex analyte enrichment strategies.[18,19,20,21,22] Therefore, there is still of great demand to develop simple, rapid and cost-effective methods that allow high-throughput access to kinetic information.

Miniaturized fluidic systems have lately emerged to address the challenges associated with present bioanalytical tools.[23] Microfluidics that offers a high degree of parallelization has the potential to increase the assay throughput while minimizing reagent consumption and analysis time. With Reynolds numbers being well below one, laminar flow has been an effective way to deliver concentration gradients of chemical species within microfluidic channels. Microfluidic diluters offer means to automatically generate stable and reproducible concentration gradients on chip for cell-based experiments,[24] pharmaceutical studies[25] and high-throughput fluorescent immunoassays.[26] Despite several successful applications, there have been a few efforts to implement gradient-generating microfluidic devices for kinetic assays. Most recently, we have reported the feasibility of using a nanofluidic fluorescence microscopy system (NFM) for low-noise real-time measurements of protein binding kinetics with optimized response time and target capture.[27] This system, relying on the combination of a functionalized nanofluidic device with a conventional fluorescence microscope, allows the generation of full kinetic sensorgrams (association and dissociation curves) with a single injection via a simple reversed flow operation. Thanks to the unique feature of nanometer scale channels, the reduced observation volume, leading to negligible levels of fluorescence background, allows the sensor surface to be directly probed without using sophisticated apparatuses such as SPR.[28]

Herein, we implement a microfluidic diluter in the NMF platform, allowing one-shot kinetic measurements to be carried out in a parallel manner on a single chip. This approach is capable of simultaneous monitoring multiple ligand surfaces through multiple analyte streams with up to ten different concentrations spanning almost 2 orders of magnitude using a single-analyte injection and without the need for lengthy surface regeneration procedure. The microfluidic diluter is employed to produce stable analyte concentration gradients within the device, thus eliminating tedious manual dilution process. In this work, generation of concentration gradients relies on diffusion-based partial mixing as described elsewhere,[29] where desired concentration gradients can be achieved by regulating the input flow rates. The microfluidic dilution network is designed such that a suitable dynamic concentration range required for kinetic studies is achieved at the outputs and the target solutions are transported through each channel at identical flow speeds. In principle, different analyte concentrations generated from the concentration diluter can be introduced over the sensors

located at independent nanochannels and the concentration-dependent binding data can be collected all at once using a bench-top fluorescence microscope and a CCD camera. We demonstrate the device performance for high-throughput measurements through kinetic studies of mouse immunoglobulin G (IgG)/anti-mouse IgG interaction.

Materials and methods

The integrated device is composed of three main components: the first component is a Y-shape microfluidic diluter, referred as the main microchannel, for the generation of partial-mixing concentration gradients; the second component is an array of 10 separated nanoslits with embedded probe-immobilized gold sensors for kinetic studies; the third component is a microchannel used for in-situ functionalization and reversed-buffer flow operation. The dimensions of each component are shown in Fig. 1. The Y-shape gradient network has two input fluid lines, one for the analyte solution with the maximum concentration for kinetic experiments, and the other for the diluent (buffer solution). Two confluent streams of liquid merge at the intersection and laterally mix via molecular diffusion in the main microchannel as they flow downstream side by side, thus generating traverse concentration gradients.

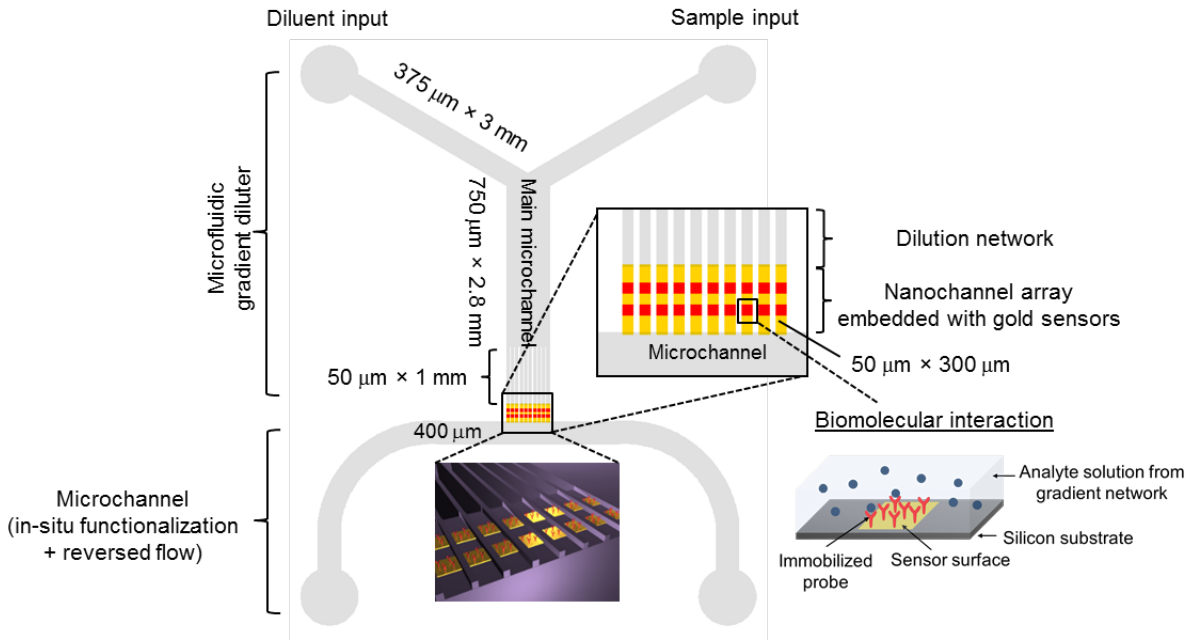

Fig. 1 Schematic representation of the concentration diluter embedded nanofluidic device used for one-shot kinetic analysis. The gradient network generates a concentration gradient of analytes that crosses over surface immobilized probes located in the nanochannel array. The Y-type diluter results in simple chip design and fabrication.

The geometry of microfluidic diluter was designed using COMSOL Multiphysics to target the desired concentration profile and flow speed (see details of the design in the ESI). After a fixed distance, the

main microchannel is partitioned into a series of 10 parallel narrow microchannels to permanently isolate and homogenize distinct sample concentrations emanating from the main flow stream before entering the nanoslits. Furthermore, the Y-shape microfluidic gradient network is symmetrical in order to guarantee the same flow velocity at all outputs, which is indispensable for parallel kinetic measurements. The flow velocity has a major influence on the steepness of the output concentration gradient profile wherein a wide sigmoidal concentration profile is obtained at a low flow velocity. Nevertheless, too high of a flow velocity can lead to non-homogeneity of the sample solutions at the exit as they do not experience enough residence time to mix while flowing along the narrow microchannels. Hence, there is a tradeoff between the concentration range generated from the gradient device and the homogeneity of the sample solution. Still, the simulation results show (see ESI) that with the selected geometry and inlet pressure, the designed Y-shape microfluidic dilution network enables gradient generation with a range of concentrations spanning approximately two orders of magnitude, and all channel outputs possessed virtually identical flow velocities.

The fluidic chip (16×16 mm^2) was fabricated on a silicon substrate using standard photolithography and reactive ion etching techniques as described previously.[27] The microfluidic channels are 10 µm deep while the nanochannels are 450 nm deep. Selective immobilization of protein receptors within the nanochannel was achieved by patterning 100 nm thick gold patches onto the silicon substrate. The functionalization protocol used to immobilize the probe molecules onto the gold sensors embedded in the nanoslits was partly carried out prior to chip encapsulation (see details in the ESI). The fluidic chip was sealed with a hard-PDMS coated cover glass using a specifically developed room-temperature bonding process.[30] The fluidic chip was then filled with a blocking solution (a buffer containing 1% bovine serum albumin and 0.02% Tween-20) to prevent nonspecific adsorption of proteins on the channel surfaces. After chip bonding and channel passivation, the functionalization of the gold sensor with protein probes was finalized in flow as described in the ESI.

The device was mounted on a dedicated fluidic support and the reservoirs were connected to a pressure controller (MFC-8C Fluigent) to induce liquid flows. All experiments were monitored using a CCD camera (ANDOR iXonEM+885) and an inverted microscope (Olympus IX70) equipped with a white light source (Lumencor SOLA light engine). Fluorescence images were acquired with a 10X microscope objective to cover an area of approximately 800 µm × 800 µm, allowing us to visualize the binding reactions in all channels.

Results and discussion

In order to investigate the effectiveness of the diluter for generating accurate concentration gradients of target solutions, we used fluorescent molecules to visualize the local concentration by means of fluorescence microscopy. A 20 nM Alexa Fluor-647 conjugated mouse anti-rabbit IgG (mIgG-AF 647) solution was injected at the analyte input port and a buffer solution at the diluent input port. To create a stable concentration gradient using the Y-type diluter, it was compulsory to maintain the pressure equilibrium between the two feeding streams at the input ports by using a single pressure source and a Y-barbed connector (Fig. 2).

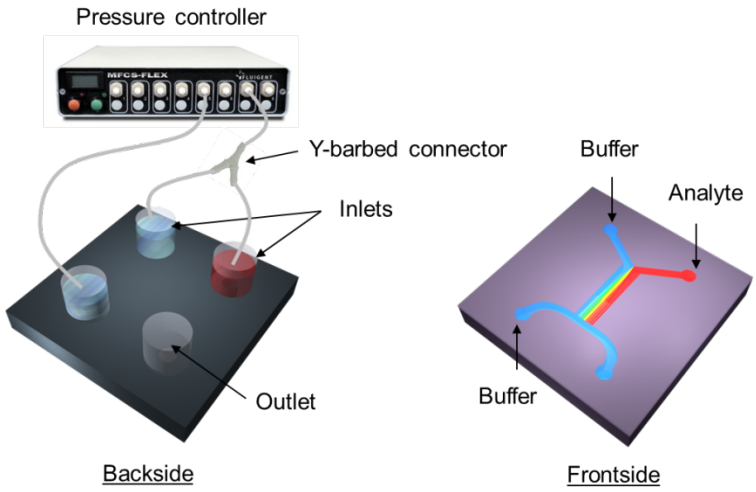

Fig. 2 Schematic diagram of the fluidic setup for the generation of analyte concentration gradients. Analyte (red color) and buffer (blue color) solutions are introduced at the inlet ports using a single pressure source and a Y-barbed connector to maintain the pressure equilibrium between two feeding streams, improving the stability of the concentration gradients within the main microchannel.

An analyte-buffer interface was observed at the stagnation point (Fig. 3a) upon injection of the mIgG-AF 647 and buffer solutions. Both fluids were mixed by molecular diffusion as they progressed down the main channel resulting in a broader fluorescence region. The concentration gradient at the end of the main channel was constantly isolated and maintained in the downstream array of narrow microchannels. It was observed that the concentration gradient was stabilized within 2 mins and controllable during the time span of the kinetic experiments (typically 10-15 min). This is particularly crucial to achieve robust and accurate kinetic information of the observed interactions. Besides, the time required to establish a steady-state equilibrium gradient was observed to be less than 1 min. This timescale is relatively short compared to the total kinetic analysis time (see next section), thus allowing the observation of the initial association phase of the binding reactions. As expected, the fluorescence intensity in the channel outputs increased from the left to the right (Fig. 3b), generating a characteristic diffusion-induced sigmoidal concentration profile[31] (error function[32]). The corresponding target concentrations were estimated by exploiting the observed linear relationship to correlate the fluorescence intensity with that of the known analyte concentration close to the inlet of the device. Fig. 3c shows the resulting plot of normalized fluorescence intensities along with the (output numbers) corresponding analyte concentrations. With an optimized flow speed at the input reservoirs, our device was capable of generating the gradients with a concentration range of approximately 2 orders of magnitude. Although this Y-type concentration diluter merely provides a sigmoidal concentration profile in the network, the generated gradient offers a sufficient number of different analyte concentrations within a suitable range for kinetic studies.

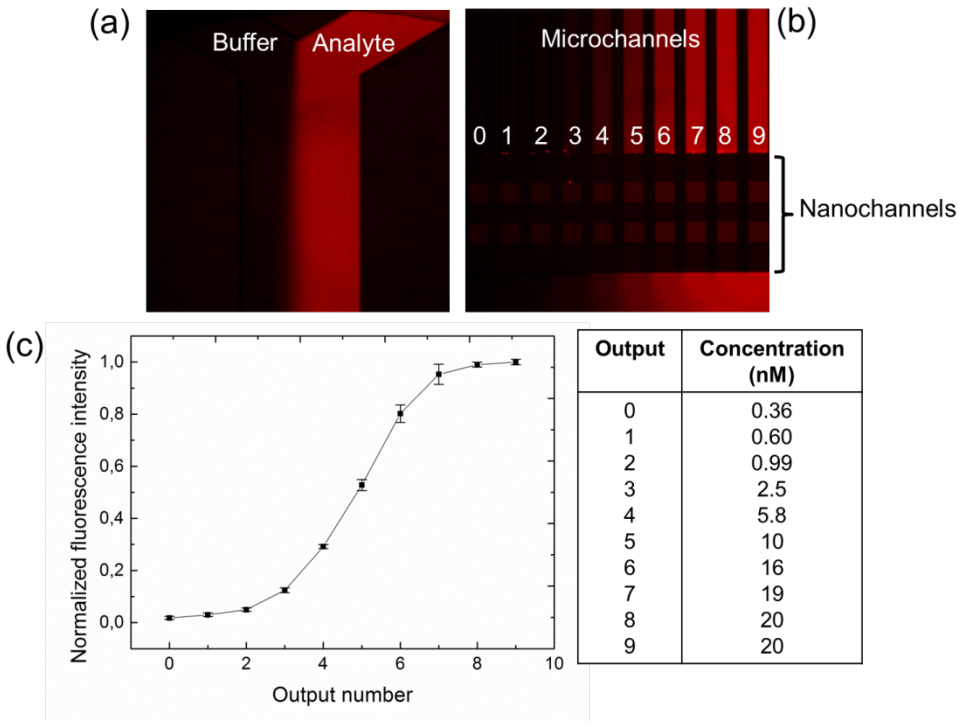

Output	Concentration (nM)
0	0.36
1	0.60
2	0.99
3	2.5
4	5.8
5	10
6	16
7	19
8	20
9	20

Fig. 3 (a) Fluorescence image at the Y-junction network where the analyte stream merges with the buffer solution. (b) Fluorescence image of ten channel outputs demonstrating the gradient dilution of analyte concentrations. (c) Plot of the normalized fluorescence intensities for all ten channels, showing a characteristic sigmoidal concentration profile. The error bars represent the fluorescence variations from 10 different regions of interest. The corresponding analyte concentrations are described in the table on the right.

To demonstrate the ability of our device to perform one-shot kinetic analysis and to yield reliable kinetic information, kinetic studies of mouse IgG (mIgG-AF 647)/anti-mouse IgG interaction were conducted. The immobilization of anti-IgG probes on the sensor surface was carried out in-situ after chip encapsulation (details of the functionalization protocol can be found in ESI). In this experiment, a 20 nM solution of mIgG-AF 647 was used as an analyte input concentration. Fluorescently labeled analytes at different concentrations produced from the concentration diluter was allowed to interact with the receptor-immobilized sensor surfaces. The binding interactions occurring in 10 separate nanoslits were observed simultaneously under the fluorescence microscope. In order to monitor the dissociation phase, the analyte flow from the Y-junction input was replaced by a reversed fluid flow from the output microchannel in order to introduce a fresh buffer solution. The total analysis time for complete kinetic experiments, including the association and dissociation steps for a full set of analyte concentrations, was approximately 20 min. This approach is therefore considerably faster than conventional kinetic studies where the total analysis time can reach several hours.

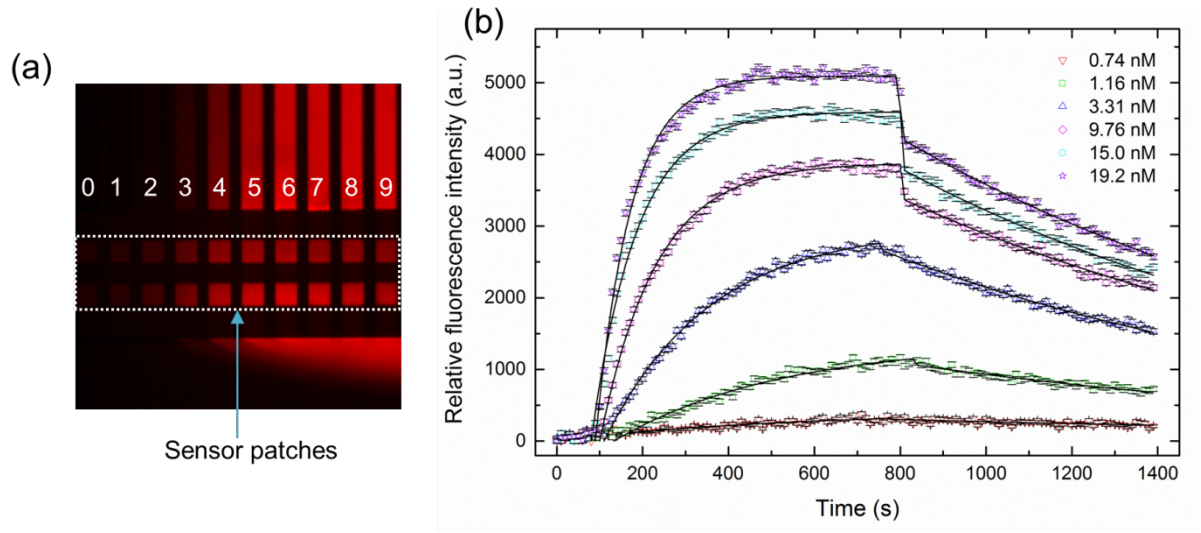

Fig. 4 (a) Fluorescence image of the observation area measured upon the binding of analytes at different concentrations with the surface immobilized probes. A mean sensor response was derived from a 4 µm × 4 µm region of interest. (b) Kinetic sensorgrams of the IgG/anti-IgG interaction for various analyte concentrations obtained from one-shot kinetic analysis with the concentration diluter integrated nanofluidic device.

The resulting gradient of concentration is shown in Fig. 4a (with estimated analyte concentrations ranging from 0.57 nM to 20 nM), along with the binding of the IgG to surface-immobilized anti-IgG. The fluorescence signals on the sensor patches gradually increase from the left channel to the right one, concomitantly with the increase in target concentration. In this study, we selected the binding data from the diluter output 1-6 that provide an adequate concentration range for curve fitting. Kinetic constant determination was carried out using an analytical well mixed model, assuming a simple 1:1 interaction and a constant and uniform analyte concentration above the sensor, similarly as in our previous work.[27] Briefly, the binding signal was selected from the regions of interest within the sensor patches for each concentration and the background signal was removed. Fig. 4b displays the kinetic sensorgrams for the IgG/anti-IgG interaction. To determine the binding constants of this interaction, the data were fitted with the well-mixed model and the plot of the apparent time constant as a function of the analyte concentration yielded a linear fit with a slope, *i.e.* an on-rate k_{on}, of 5.3±0.3 × 10^5 $M^{-1}s^{-1}$ (R^2 = 0.9909, plot not shown). The dissociation constant was extracted by fitting the dissociation curves with a first-order exponential decay and the average off-rate constant k_{off} was found to be 7.8±0.9 × 10^{-4} s^{-1}. This gives the equilibrium dissociation constant (*KD*) of 1.5 nM. These values are in the same order of magnitude as those measured in a sequential fashion with our NFM platform (i.e. k_{on} = 6.0±0.3 × 10^5 $M^{-1}s^{-1}$; k_{off} = 5.5±0.4 × 10^{-4} s^{-1}; *KD* = 0.92 nM)[27] and those reported earlier using conventional kinetic experiments.[33,34]

Conclusions

We have demonstrated a convenient, simple and effective on-chip concentration diluter-based nanofluidic fluorescence microscopy for parallel kinetic studies of biomolecular interactions. This

represents the first application of one-shot kinetic analysis on a nanofluidic biosensor platform. A mouse IgG/anti-mouse IgG interaction model was used to evaluate the effectiveness of the integrated device. The results show that our system is capable of performing parallel kinetic measurements on a single device, providing accurate and high-throughput access to kinetic information of protein interactions. Since the surface regeneration is not required, this approach offers time-saving assays (~ 10 times) and substantial reduction of reagent consumption (~ 1000 times) as compared to traditional kinetic experiments, such as in SPR setup. It is expected that this innovative technology will open up new opportunities for improved high-throughput screening in drug discovery and real-time protein interaction arrays.

Acknowledgements

We are grateful to Sandrine Geoffroy, Laboratoire Matériaux et Durabilité des Constructions (LMDC), Toulouse, for her helpful discussion. The authors acknowledge the Programme Blanc jointly sponsored by the Agence Nationale de la Recherche (ANR-13-IS10-0001) and the Ministry of Science and Technology, Taiwan (103-2923-M-001-007-MY3), and the MAE (Ministère des Affaires Etrangères) for the doctoral fellowship of P.T. This work was partly supported by the French RENATECH Network, Academia Sinica Integrated Thematic Project (AS-106-TP-A03), and AOARD grant #134023.

References

1. Andersson, K., Karlsson, R., Löfås, S., Franklin, G. & Hämäläinen, M. D. Label-free kinetic binding data as a decisive element in drug discovery. *Expert Opin. Drug Discov.* **1,** 439–446 (2006).
2. Fägerstam, L. G., Frostell-Karlsson, A., Karlsson, R., Persson, B. & Rönnberg, I. Biospecific interaction analysis using surface plasmon resonance detection applied to kinetic, binding site and concentration analysis. *J. Chromatogr.* **597,** 397–410 (1992).
3. Rich, R. L., Quinn, J. G., Morton, T., Stepp, J.D. & Myszka, D. G. Biosensor-based fragment screening using FastStep injections. *Anal. Biochem.* **407,** 270–7 (2010).
4. Quinn, J. G. Modeling Taylor dispersion injections: determination of kinetic/affinity interaction constants and diffusion coefficients in label-free biosensing. *Anal. Biochem.* **421,** 391–400 (2012).
5. Chavanieu, A. & Pugnière, M. Developments in SPR Fragment Screening. *Expert Opin Drug Discov.* **11,** 489-99 (2016).
6. Nahsol, O. *et al.* Parallel kinetic analysis and affinity determination of hundreds of monoclonal antibodies using the ProteOn XPR36. *Anal. Biochem.* **383,** 52–60 (2008).
7. Rich, R. L. *et al.* Extracting kinetic rate constants from surface plasmon resonance array systems. *Anal. Biochem.* **373,** 112–120 (2008).
8. Patching, S. G. Surface plasmon resonance spectroscopy for characterisation of membrane protein ligand interactions and its potential for drug discovery. *Biochim. Biophys. Acta.* **1838,** 43–55 (2014).

9. Maynard, J. A., Lindquist, N. C., Sutherland, J. N., Lesuffleur, A., Warrington, A. E., Rodriguez, M. & Oh, S. H. Surface plasmon resonance for high-throughput ligand screening of membrane-bound proteins. *Biotechnol. J*. **4,** 1542–58 (2009).
10. Homola, J., Yee, S. S. & Myszka, D. Chapter 4 – Surface plasmon resonance biosensors, in *Optical Biosensors (Second Edition)* 185–242 (Elsevier, 2008).
11. Labib, M., Sargent, E. H., Kelley, S. O. Electrochemical Methods for the Analysis of Clinically Relevant Biomolecules. *Chemical Reviews* **116**, 9001-9090 (2016).
12. Swami, N. S., Chou, C. F. & Terberueggen, R. Two-potential electrochemical probe for study of DNA immobilization. *Langmuir* **21**, 1937-1941 (2005).
13. O'Sullivan, C. K., Guilbault, G. G. Commercial quartz crystal microbalances - theory and applications. *Biosensors & Bioelectronics* **14**, 663-670 (1999).
14. Liu, Y., Yu, X., Zhao, R., Shangguan, D. H., Bo, Z. Y. & Liu, G. Q. Real time kinetic analysis of the interaction between immunoglobulin G and histidine using quartz crystal microbalance biosensor in solution. *Biosensors & Bioelectronics* **18**, 1419-1427 (2003).
15. Sanghavi, B. J., Sitaula, S., Griep, M. H., Karna, S. P., Ali, M. F., & Swami N. S. Real-Time Electrochemical Monitoring of Adenosine Triphosphate in the Picomolar to Micromolar Range Using Graphene-Modified Electrodes. *Analytical Chemistry* **85**, 8158-8165 (2013).
16. Gao, Y., Wolf, L. K. & Georgiadis, R. M. Secondary structure effects on DNA hybridization kinetics: a solution versus surface comparison. *Nucleic Acids Research* **34**, 3370-3377 (2006).
17. Wei, C. W., Cheng, J. Y., Huang, C. T., Yen, M. H. & Young, T. H. Using a microfluidic device for 1 µl DNA microarray hybridization in 500 s. *Nucleic Acids Research* **33**, (2005).
18. Swami, N., Chou, C. F., Ramamurthy, V. & Chaurey, V. Enhancing DNA hybridization kinetics through constriction-based dielectrophoresis. *Lab on a Chip* **9**, 3212-3220 (2009).
19. Liao, K. T. & Chou, C. F. Nanoscale Molecular Traps and Dams for Ultrafast Protein Enrichment in High-Conductivity Buffers. *Journal of the American Chemical Society* **134**, 8742-8745 (2012).
20. Liao, K. T., Tsegaye, M., Chaurey, V., Chou, C. F. & Swami, N. S. Nano-constriction device for rapid protein preconcentration in physiological media through a balance of electrokinetic forces. *Electrophoresis* **33**, 1958-1966 (2012).
21. Chaurey, V., Rohani, A., Su, Y. H., Liao, K. T., Chou, C. F. & Swami, N. S. Scaling down constriction-based (electrodeless) dielectrophoresis devices for trapping nanoscale bioparticles in physiological media of high-conductivity. *Electrophoresis* **34**, 1097-1104 (2013).
22. Bercovici, M., Han, C. M., Liao, J. C. & Santiago, J. G. Rapid hybridization of nucleic acids using isotachophoresis. *Proceedings of the National Academy of Sciences of the United States of America* **109**, 11127-11132 (2012).
23. Khandurina, J. & Guttman, A. Bioanalysis in microfluidic devices. *J. Chromatogr. A* **943,** 159–183 (2002).
24. Chung, B. G. *et al.* Human neural stem cell growth and differentiation in a gradient-generating microfluidic device. *Lab. Chip* **5,** 401–406 (2005).
25. Pihl, J. *et al.* Microfluidic gradient-generating device for pharmacological profiling. *Anal. Chem.* **77,** 3897–3903 (2005).
26. Jiang, X., Ng, J. M. K., Stroock, A. D., Dertinger, S. K. W. & Whitesides, G. M. A miniaturized, parallel, serially diluted immunoassay for analyzing multiple antigens. *J. Am. Chem. Soc.* **125,** 5294–5295 (2003).
27. Teerapanich, P. *et al.* Nanofluidic Fluorescence Microscopy (NFM) for real-time monitoring of protein binding kinetics and affinity studies. *Biosens. Bioelectron.* **88,** 25–33 (2017).

28. Leïchlé, T. & Chou, C.-F. Biofunctionalized nanoslits for wash-free and spatially resolved real-time sensing with full target capture. *Biomicrofluidics* **9,** 034103 (2015).
29. Holden, M. A., Kumar, S., Castellana, E. T., Beskok, A. & Cremer, P. S. Generating fixed concentration arrays in a microfluidic device. *Sens. Actuators B Chem.* **92,** 199–207 (2003).
30. Leïchlé, T. *et al.* Biosensor-compatible encapsulation for pre-functionalized nanofluidic channels using asymmetric plasma treatment. *Sens. Actuators B Chem.* **161,** 805–810 (2012).
31. Crank, J. The mathematics of diffusion, Oxford University Press, Second edi., 1975.
32. Salmon, J.-B., Ajdari, A., Tabeling, P., Servant, L., Talaga, D. & Joanicot, M. In situ Raman imaging of interdiffusion in a microchannel. *Appl. Phys. Lett.* **86**, 094106 (2005).
33. Yu, C.-J. *et al.* Fiber optic biosensor for monitoring protein binding kinetics. *Proc SPIE* **5691,** 200–208 (2005).
34. Sapsford, K. E., Liron, Z., Shubin, Y. S. & Ligler, F. S. Kinetics of antigen binding to arrays of antibodies in different sized spots. *Anal. Chem.* **73,** 5518–5524 (2001).